HHS Public Access

Author manuscript

Nat Med. Author manuscript; available in PMC 2016 May 18.

Published in final edited form as:

Nat Med. 2015 December ; 21(12): 1464–1472. doi:10.1038/nm.3974.

The TAM receptor Mertk protects against neuroinvasive viral infection by maintaining blood-brain barrier integrity

Jonathan J. Miner[1], **Brian P. Daniels**[2], **Bimmi Shrestha**[1], **Jose L. Proenca-Modena**[1,6], **Erin D. Lew**[7], **Helen M. Lazear**[1], **Matthew J. Gorman**[4], **Greg Lemke**[7], **Robyn S. Klein**[1,2,4], and **Michael S. Diamond**[1,3,4,5,*]

[1]Department of Medicine, Washington University School of Medicine, Saint Louis, MO 63110.

[2]Department of Anatomy and Neurobiology, Washington University School of Medicine, Saint Louis, MO 63110.

[3]Department of Molecular Microbiology, Washington University School of Medicine, Saint Louis, MO 63110.

[4]Department of Pathology and Immunology, Washington University School of Medicine, Saint Louis, MO 63110.

[5]The Center for Human Immunology and Immunotherapy Programs, Washington University School of Medicine, Saint Louis, MO 63110.

[6]Department of Genetics, Evolution and Bioagents, Institute of Biology, University of Campinas (UNICAMP), Campinas, SP, Brazil

[7]Molecular Neurobiology Laboratory, The Salk Institute, La Jolla, California 92037.

Abstract

The TAM receptors Tyro3, Axl, and Mertk are receptor tyrosine kinases that dampen host innate immune responses following engagement with their ligands, Gas6 and Protein S, which recognize phosphatidylserine on apoptotic cells. In a form of apoptotic mimicry, many enveloped viruses display phosphatidylserine on the outer leaflet of their membranes, enabling TAM receptor activation and down-regulation of antiviral responses. Accordingly, we hypothesized that a deficiency of TAM receptors would enhance antiviral responses and protect against viral infection. Unexpectedly, mice lacking Mertk and/or Axl but not Tyro3 exhibited greater vulnerability to infection with neuroinvasive West Nile and La Crosse viruses. This phenotype was associated with increased blood-brain barrier permeability, which enhanced virus entry into and infection of the

*Address correspondence to: Michael S. Diamond, M.D. Ph.D., Departments of Medicine, Molecular Microbiology, and Pathology and Immunology, Washington University School of Medicine, 660 South Euclid Ave. Box 8051, Saint Louis, MO 63110, USA. ; Email: diamond@borcim.wustl.edu, (314) 362-2842

AUTHOR CONTRIBUTIONS

J.J.M., B.P.D., H.M.L., G.L., R.S.K., and M.S.D. designed the experiments. J.J.M., B.P.D., B.S., J.L.P-M., H.M.L., and M.J.G. performed the experiments. E.L. and G.L. contributed essential reagents. J.J.M. and M.S.D. wrote the initial draft of the manuscript, with all other authors providing critical comments and editorial changes.

CONFLICT OF INTEREST STATEMENT

The authors have no conflicts of interest to disclose.

brain. Activation of Mertk synergized with IFN-β to tighten cell junctions and prevent virus transit across brain microvascular endothelial cells. Because TAM receptors restrict pathogenesis of neuroinvasive viruses, these findings have implications for TAM antagonists that are currently in clinical development.

INTRODUCTION

The TAM receptors Tyro3, Axl, and Mertk have pleiotropic functions in cancer metastasis, angiogenesis, thrombus stabilization, and innate immune regulation[1,2]. Axl and/or Mertk are expressed on cells involved in immune control and trafficking, including macrophages, dendritic cells (DCs), platelets, and endothelial cells[1]. In comparison, Tyro3 expression is prominent on central nervous system (CNS) neurons[3]. TAM receptors signal upon recognition of their phosphatidylserine-bound ligands, Gas6 and Protein S[4]. The consequences of TAM signaling depend on cell type. For example, TAM receptors are important for NK cell development[5], and their inhibition may license NK cells to reject metastatic tumors[6]. Axl and Mertk signaling in endothelial cells modulates angiogenesis[7-9], whereas their signaling in platelets promotes thrombus stabilization[10]. In DCs, activation of Axl down-regulates production and signaling of pro-inflammatory cytokines by interacting physically with the R1 subunit of the type I interferon (IFN) receptor (IFNAR1) to promote expression of the negative regulators SOCS1 and SOCS3[11]. The TAM receptors also have essential roles in clearance of apoptotic cells by macrophages, retinal pigment epithelial cells, and other professional phagocytes[12-14]. The TAM ligands Gas6 and Protein S physically bridge a TAM receptor expressed on the surface of a phagocyte to phosphatidylserine expressed on the surface of the apoptotic cell.

TAM receptors are therapeutic targets in cancer because of their effects on tumor angiogenesis, NK cell licensing, tumor cell survival, metastasis, and immune suppression in tumor-associated macrophages[6-9]. Several antagonists and blocking antibodies are under evaluation in clinical trials[15,16]. TAM receptor agonists also may prove useful in the treatment of autoimmunity because of their ability to down-regulate cytokine production[17]. Less is known about the net effect of TAM receptor blockade during viral infection. In a form of apoptotic mimicry, many enveloped viruses incorporate phosphatidylserine into their virion membranes[18,19] and bind Gas6 and Protein S to facilitate recognition by TAM receptors and activation of signals that dampen antiviral responses[19]. Studies with influenza and respiratory syncytial viruses suggest that Axl blockade by antibodies protects against infection and disease pathogenesis[20]. However, an antiviral phenotype after TAM inhibition may not be universal, as herpes simplex virus (HSV) infection was more severe in *Axl*$^{-/-}$ mice[21].

We hypothesized that deletion of TAM receptors might restrict WNV infection and protect against pathogenesis for two reasons: (1) cell culture studies indicated that TAM receptors can augment flavivirus entry[18] and create a more permissive innate immune environment for replication[19]; and (2) WNV causes significant morbidity in humans after it crosses the blood-brain barrier (BBB) and replicates within neurons. Type I IFN signaling strengthens the BBB during viral infection by tightening junctions between brain microvascular

endothelial cells (BMECs)[22]. Since TAM receptors can negatively regulate type I IFN signaling[11,19], deletion of TAM receptors could enhance both IFN signaling and BBB integrity. Unexpectedly, we observed that *Axl*$^{-/-}$, *Mertk*$^{-/-}$, *Axl*$^{-/-}$*Mertk*$^{-/-}$ but not *Tyro3*$^{-/-}$ mice were more vulnerable to WNV infection. This phenotype was associated with markedly impaired BBB integrity during infection. Our results establish a preferential role for Mertk in protecting against neuroinvasive viruses, which occurs at least in part through its ability to sustain the BBB during infection.

RESULTS

Axl and Mertk but not Tyro3 are required for control of WNV infection in vivo

To evaluate the role of TAM receptors in WNV infection, we infected WT, *Tyro3*$^{-/-}$, *Axl*$^{-/-}$, *Mertk*$^{-/-}$, and *Axl*$^{-/-}$*Mertk*$^{-/-}$ C57BL/6 mice with WNV (New York 2000 strain) by subcutaneous inoculation (**Fig 1a**). Unexpectedly, *Axl*$^{-/-}$, *Mertk*$^{-/-}$, and *Axl*$^{-/-}$*Mertk*$^{-/-}$, but not *Tyro3*$^{-/-}$ mice were more vulnerable to WNV infection than WT mice, with ~80% mortality in *Axl*$^{-/-}$ or *Mertk*$^{-/-}$ mice ($P < 0.0005$) and ~95% mortality in *Axl*$^{-/-}$*Mertk*$^{-/-}$ mice ($P < 0.0005$).

We found that an absence of TAM receptors had a relatively minor effect on viral burden in peripheral organs, with increased viremia and viral load observed only at 2 days post-infection (dpi) in serum (26-fold, $P < 0.05$) and 4 dpi in the spleen (33-fold, $P < 0.05$), respectively, in the *Axl*$^{-/-}$*Mertk*$^{-/-}$ mice (**Fig 1b–c**). No significant differences in viral burden were observed in serum, spleen, or kidney in *Axl*$^{-/-}$ or *Mertk*$^{-/-}$ mice compared to WT mice (**Fig 1b–d**).

Higher levels of WNV infection were apparent in the CNS of *Axl*$^{-/-}$, *Mertk*$^{-/-}$, and *Axl*$^{-/-}$*Mertk*$^{-/-}$ mice compared to WT controls. At 4 dpi, WNV was detected in CNS tissues of TAM receptor deficient mice: 2 of 9 *Axl*$^{-/-}$, 2 of 10 *Mertk*$^{-/-}$, and 3 of 10 *Axl*$^{-/-}$ *Mertk*$^{-/-}$ mice had brain homogenates that were positive for infectious WNV compared to 0 of 10 WT mice (**Fig 1e**). Analogously, at 6 dpi, 5 of 9 *Axl*$^{-/-}$, 4 of 8 *Mertk*$^{-/-}$, and 4 of 9 *Axl*$^{-/-}$*Mertk*$^{-/-}$ mice had detectable WNV in the spinal cord compared to 0 of 10 WT mice (**Fig 1f**). Viral titers also were increased at 8 dpi in the brain (29 to 72-fold increase, $P < 0.05$) and spinal cord (7 to 135-fold increase, $P < 0.05$) of *Axl*$^{-/-}$, *Mertk*$^{-/-}$, and *Axl*$^{-/-}$ *Mertk*$^{-/-}$ mice.

Higher levels of CNS infection in the TAM receptor KO animals could suggest that Axl or Mertk restrict viral replication preferentially in target cells of the CNS. To test this hypothesis, we inoculated WNV intracranially in *Axl*$^{-/-}$, *Mertk*$^{-/-}$, or *Tyro3*$^{-/-}$ mice. To ensure detection of small differences that might be missed by whole brain analysis, viral burden in the cerebral cortex, subcortex, brain stem, and cerebellum was measured at 3, 5, and 6 dpi after infection. However, no difference in viral burden in the CNS of *Axl*$^{-/-}$, *Mertk*$^{-/-}$, or *Tyro3*$^{-/-}$ mice was observed following intracranial inoculation (**Fig 1g–i,** $P > 0.9$). These data suggest that TAM receptors do not restrict WNV replication directly in the CNS.

Effects of TAM receptors on antiviral adaptive immune responses

To assess whether part of the CNS virological phenotype could be attributed to defects in adaptive immunity, we measured anti-WNV IgM and IgG levels at 4 and 8 dpi in WT and *Axl*$^{-/-}$*Mertk*$^{-/-}$ mice (**Supplementary Fig 1a–c**). *Axl*$^{-/-}$*Mertk*$^{-/-}$ mice had slightly greater anti-WNV IgG titers (2.5-fold, $P < 0.005$) and slightly lower neutralizing titers at 8 dpi (0.4-fold, $P < 0.005$). These small differences were unlikely to explain the prominent lethality phenotype observed in *Axl*$^{-/-}$*Mertk*$^{-/-}$ mice after WNV infection.

Axl has been proposed to modulate CD8$^+$ T cell responses by DC efferocytosis and antigen cross-presentation[21]. To test whether Axl and Mertk affected T cell responses during WNV infection, we measured the levels and antigen specificity of CD8$^+$ T cells from the spleen of WNV-infected WT, *Axl*$^{-/-}$, *Mertk*$^{-/-}$ and *Axl*$^{-/-}$*Mertk*$^{-/-}$ mice (**Supplementary Fig 1d–n**). Although we detected similar numbers and percentages of CD4$^+$ and CD8$^+$ T cells in the spleens of WT, *Axl*$^{-/-}$, *Mertk*$^{-/-}$ and *Axl*$^{-/-}$*Mertk*$^{-/-}$ mice at 8 dpi, we observed fewer WNV tetramer-positive CD8$^+$ T cells in *Axl*$^{-/-}$ mice (**Supplementary Fig 1d–f**). After *ex vivo* peptide restimulation of splenocytes, we observed a lower percentage and number of WNV-specific CD8$^+$ T cells that expressed IFN-γ in *Axl*$^{-/-}$ but not in *Mertk*$^{-/-}$ CD8$^+$ T cells (**Supplementary Fig 1k–l**, $P < 0.05$). There also were fewer WNV-specific CD8$^+$ T cells that expressed IFN-γ or TNF-α from *Axl*$^{-/-}$*Mertk*$^{-/-}$ mice (**Supplementary Fig 1m–n**, $P < 0.05$). These data suggest that Axl is required for optimal priming of a CD8$^+$ T cell response during WNV infection.

We next assessed leukocyte responses within the brain at 8 dpi. We observed greater numbers of leukocytes and antigen-specific CD8$^+$ T cells in the brains of *Mertk*$^{-/-}$ and *Axl*$^{-/-}$*Mertk*$^{-/-}$ mice than WT controls (**Supplementary Fig 2a–g**, $P < 0.05$) but no statistically significant difference in the number of CD11b$^+$CD45^{hi} macrophages or CD11b$^+$CD45^{lo} microglia (**Supplementary Fig 2h–i**). Greater numbers of infiltrating immune cells likely result from the higher viral burden in the CNS, enhanced BBB permeability, or both.

BBB integrity during WNV infection requires Axl and Mertk but not Tyro3

Because we observed early accumulation of WNV in the brains of *Axl*$^{-/-}$, *Mertk*$^{-/-}$, and *Axl*$^{-/-}$*Mertk*$^{-/-}$ mice, we assessed whether these mice had altered BBB permeability that could impact virus entry into the CNS. We injected sodium fluorescein (molecular weight (MW): 376) intraperitoneally into naïve and WNV-infected WT, *Tyro3*$^{-/-}$, *Axl*$^{-/-}$, *Mertk*$^{-/-}$, and *Axl*$^{-/-}$*Mertk*$^{-/-}$ mice and measured extravasation into the brain 45 minutes later (**Fig 2a**). Even in the absence of infection, naïve *Axl*$^{-/-}$*Mertk*$^{-/-}$ mice had slightly greater BBB permeability; in comparison, no statistically significant differences were observed in naïve *Tyro3*$^{-/-}$, *Axl*$^{-/-}$, *or Mertk*$^{-/-}$ mice, although there was a trend toward enhanced BBB permeability in uninfected *Mertk*$^{-/-}$ mice (**Fig 2a**, *left panel*). WNV infection resulted in increased sodium fluorescein extravasation into the CNS at 4 dpi (**Fig 2a,** *right panel*), as reported previously[22]. BBB permeability was greater in WNV-infected *Axl*$^{-/-}$, *Mertk*$^{-/-}$, and *Axl*$^{-/-}$*Mertk*$^{-/-}$, but not *Tyro3*$^{-/-}$ mice compared to WT mice at this time point, with *Mertk*$^{-/-}$ and *Axl*$^{-/-}$*Mertk*$^{-/-}$ mice exhibiting the most pronounced phenotypes (**Fig 2a**, *right panel*). These results suggest that Axl and Mertk are required to maintain BBB integrity

during infection and prevent early virus invasion into the CNS, with Mertk having the most prominent effect.

As an independent measure of BBB permeability, we used confocal microscopy to assess leakage of endogenous IgG (MW: 150,000) into the brain parenchyma following WNV infection. Although minimal IgG was detected in the brains of uninfected mice corresponding to all genotypes (data not shown), IgG accumulation became apparent at 4 dpi, with $Axl^{-/-}Mertk^{-/-}$ mice exhibiting greater leakage than WT mice (**Fig 2b**). Thus, in the context of WNV infection, the BBB of $Axl^{-/-}Mertk^{-/-}$ mice was more permeable to small molecules and larger proteins.

TAM antagonist disrupts BBB integrity and accelerates WNV infection in the brain

To corroborate the phenotypes observed with TAM receptor KO mice, we treated WT mice with a 40 mg/kg dose of BMS-777607, a small molecule inhibitor of c-Met, Ron, Flt-3, and TAM receptor signaling[23], by oral gavage beginning one day prior to WNV infection and continuing until 4 dpi. BMS-777607 treatment resulted in enhanced lethality of WT mice after WNV infection (**Supplementary Fig 3a**, $P < 0.05$) with virus present in the brain at 4 dpi in 3 of 6 drug-treated mice compared to 0 of 6 control mice (**Supplementary Fig 3b**). BMS-777607 increased BBB permeability in WT but not $Axl^{-/-}$ $Mertk^{-/-}$ mice at 4 dpi (**Supplementary Fig 3c** $P < 0.05$), nor in drug-treated uninfected animals (**Supplementary Fig 3d**).

TAM receptor KO mice are vulnerable to La Crosse virus infection

We hypothesized that $Mertk^{-/-}$ mice also might be vulnerable to other viruses that enter the brain through a hematogenous route. La Crosse virus (LACV) is a neurotropic orthobunyavirus that causes meningoencephalitis, predominantly in children[24]. We observed enhanced mortality in $Axl^{-/-}$ or $Mertk^{-/-}$ mice infected with LACV compared to WT mice (**Fig 3a**, 50% versus 9%, $P < 0.05$). $Mertk^{-/-}$ mice had increased BBB permeability at 4 dpi whereas LACV-infected $Axl^{-/-}$ mice did not (**Fig 3b**). We also found higher levels of viral RNA in the brains of $Mertk^{-/-}$ but not $Axl^{-/-}$ mice at 8 dpi (**Fig 3c**) after LACV infection.

Cytokine and chemokine levels in serum of WNV-infected mice

Elevated levels of some pro-inflammatory cytokines (*e.g.,* TNF-α) open the BBB[25], whereas others (*e.g.,* type I IFN) close the barrier[22]. Because TAM receptors negatively regulate cytokine production, we measured their levels in the serum of naïve and WNV-infected mice (**Supplementary Fig 4**). In naïve mice, $Axl^{-/-}$, $Mertk^{-/-}$, and $Axl^{-/-}Mertk^{-/-}$ mice had higher levels of IL12-p40 although other pro-inflammatory cytokines were similar compared to WT animals. At 4 dpi, levels of TNF-α, IL-1β, IL-6, IL-12(p40), RANTES, and KC were slightly (~2-to-3 fold, $P < 0.05$) higher in the serum of $Axl^{-/-}$, $Mertk^{-/-}$, and $Axl^{-/-}Mertk^{-/-}$ mice (**Supplementary Fig 4a–g**). Type I IFN levels in serum also were slightly higher at 4 dpi in $Axl^{-/-}$ and $Axl^{-/-}Mertk^{-/-}$ mice (1.3- to 1.5-fold $P < 0.05$) but not in $Mertk^{-/-}$ mice ($P > 0.9$) (**Supplementary Fig 4h**).

We also assessed cytokine levels in the brains of $Axl^{-/-}$, $Mertk^{-/-}$, and $Axl^{-/-}Mertk^{-/-}$ mice that were inoculated via intracranial injection with WNV (**Supplementary Fig 4i**) in order

to measure cytokine expression levels in the context of equivalent WNV burden in WT and TAM receptor-deficient mice (see **Fig 1g–i**). We found no difference in expression of TNF-α, IL-1β, IL-6, TGF-β1 and TGF-β3 mRNA among any of the genotypes. Consistent with this finding, antibody blockade of TNF-α *in vivo* did not change the BBB permeability defect in *Axl*$^{-/-}$*Mertk*$^{-/-}$ mice during WNV infection (data not shown). The net effect of differences in levels of pro-inflammatory cytokines on BBB permeability in TAM receptor-deficient mice remains unclear.

Axl and Mertk signaling improves BBB integrity in vitro

TAM receptors are present on the surface of mouse BMECs *in vivo* and *in vitro*, with higher expression of Mertk compared to Axl[26,27] (**Supplementary Fig 5a–c**). To explore whether TAM receptor signaling modulates endothelial barrier integrity and WNV transit, we used an *in vitro* model of the BBB[22]. Primary mouse BMECs are cultured in the upper chamber of a transwell, with primary astrocytes in the lower chamber. Transendothelial electrical resistance (TEER) across the BMEC monolayer measures barrier integrity, with higher resistance indicating a tighter barrier. TEER was lower across *Axl*$^{-/-}$*Mertk*$^{-/-}$ BMECs (**Fig 4a**, $P < 0.05$) at baseline. In response to WNV infection, and as expected, WT and *Axl*$^{-/-}$*Mertk*$^{-/-}$ BMEC barriers exhibited increased TEER compared with mock-infected barriers, but *Axl*$^{-/-}$*Mertk*$^{-/-}$ BMEC barriers failed to tighten as much as WT BMECs (**Fig 4a–b**, 0.85-fold, $P < 0.0001$). We observed no difference in WT and *Axl*$^{-/-}$*Mertk*$^{-/-}$ BMEC viability (data not shown).

We next evaluated whether changes in TEER in *Axl*$^{-/-}$*Mertk*$^{-/-}$ BMECs impacted transit of WNV across the endothelial barrier. We added WNV to the upper chamber and after 6 h measured virus that had crossed the BMEC barrier into the lower chamber; this time point precedes *de novo* spread of WNV infection[28]. Consistent with lower TEER, *Axl*$^{-/-}$*Mertk*$^{-/-}$ BMECs had higher amounts (9-fold, $P < 0.0001$) of WNV crossing into the lower chamber compared to WT cells (**Fig 4c**). Higher levels of WNV in the lower chamber could result from decreased binding of WNV to BMECs in the absence of Axl and Mertk, since these receptors are engaged by WNV at the plasma membrane[18]. However, we found slightly higher amounts of WNV associated with BMECs lacking Axl and Mertk expression at 6 h after infection (**Fig 4d).** Thus, Axl and Mertk are not required for binding of WNV to BMECs, and TAM receptor signaling sustains the integrity of the endothelial barrier, which restricts WNV transit.

The decrease in TEER in response to WNV infection in *Axl*$^{-/-}$*Mertk*$^{-/-}$ BMECs might be due to an altered production or response to cytokines (*e.g.,* TNF-α), which independently affect the barrier. Indeed, we detected slightly increased levels (1.4- to 2.6-fold $P < 0.05$) of TNF-α, IL-1β, and IFN-γ during WNV infection of BMECs (**Fig 4e–f,** and data not shown). Other cytokine and chemokine levels (*e.g.*, IL-2, IL-3, IL-6, IL-13, KC, MIP1α, RANTES) were similar in WT and BMECs (data not shown). Since TNF-α and IL-1β can disrupt BBB integrity[22], we tested whether blockade of these cytokines *in vitro* during WNV infection might differentially alter barrier integrity. Treatment of BMECs with blocking antibodies against IL-1β and TNF-α prior to infection minimally increased TEER (1.1 to 1.2-fold, $P < 0.05$) in both WT and *Axl*$^{-/-}$*Mertk*$^{-/-}$ BMECs, and this effect was evident only at late time

points (**Fig 4g**). As studies have suggested that TAM receptors can modulate the responsiveness of endothelial cells to TNF-α[22], we treated WT and *Axl*$^{-/-}$*Mertk*$^{-/-}$ BMECs with soluble TNF-α; however no difference in TEER was observed ($P > 0.9$, **Fig 4h**).

As Axl associates physically with IFNAR1 and modulates type I IFN signaling in DCs[11], we hypothesized that TAM receptors might affect IFNAR signaling in BMECs, which could affect BBB tightening after WNV infection. To test this idea, we treated WT or *Axl*$^{-/-}$*Mertk*$^{-/-}$ BMECs with IFN-β (IFNAR-dependent) or IFN-λ (IFNAR-independent) and measured TEER over 6 hours. Whereas a deficiency of Axl and Mertk did not affect the ability of IFN-λ to increase TEER[22,29], *Axl*$^{-/-}$*Mertk*$^{-/-}$ BMECs were less responsive to IFN-β treatment in terms of TEER changes (**Fig 4i**), although IFNAR expression was similar in WT and *Axl*$^{-/-}$*Mertk*$^{-/-}$ BMECs (**Supplementary Fig 5d**). These results suggest that Axl and Mertk expression in BMECs is required for the full effect on barrier integrity of IFN-β. Colocalization of the tight junction (TJ) proteins claudin-5 and ZO-1 is enhanced by type I IFN during WNV infection[22]. We observed diminished claudin-5 expression at the cell membrane in addition to discontinuities in TJs in *Axl*$^{-/-}$*Mertk*$^{-/-}$ BMECs (**Fig 4j**). Treatment of WT and *Axl*$^{-/-}$*Mertk*$^{-/-}$ BMECs with IFN-β or IFN-λ enhanced ZO-1 and claudin-5 colocalization in WT and *Axl*$^{-/-}$*Mertk*$^{-/-}$ BMECs, although discontinuities in TJs were still observed in *Axl*$^{-/-}$*Mertk*$^{-/-}$ BMECs. In contrast, treatment with TNF-α disrupted TJ in both WT and *Axl*$^{-/-}$*Mertk*$^{-/-}$ BMECs. Diminished TJ integrity, increased virus transit, and altered IFN-β responsiveness in *Axl*$^{-/-}$*Mertk*$^{-/-}$ BMECs may explain how endothelial cell expression of TAM receptors can enhance BBB integrity during viral infection.

We next tested the effects of Gas6[4], which binds to and activates both Axl and Mertk, either alone or in combination with IFN-β, on TEER in WT BMECs. We observed dose-dependent tightening of BMEC monolayers in response to Gas6 (**Fig 5a**). The combination of Gas6 and IFN-β rapidly tightened the barrier, with markedly increased TEER values observed within 15 min of treatment. Similar increases in TEER values were observed in a human BMEC line and with physiologic concentrations of Protein S, which functions as a ligand for Mertk and Tyro3 but not Axl[4] (**Supplementary Fig 6a–b**). Consistent with its dominant role in maintaining BBB integrity *in vivo* (see **Fig 2a and 3b**), signaling through Mertk was required for the increase in TEER in response to Gas6 (**Fig 5d**). Whereas *Tyro3*$^{-/-}$ and *Axl*$^{-/-}$ BMECs responded to Gas6 similarly compared to WT cells (**Fig 5b–c**), *Axl*$^{-/-}$ BMECs exhibited decreased baseline TEER (**Fig 5c**). A combined genetic deficiency of *Axl*$^{-/-}$ and *Mertk*$^{-/-}$ did not increase the barrier defect beyond that observed in *Mertk*$^{-/-}$ BMECs in response to Gas6 and IFN-β (**Fig 5d–e**).

To investigate further the interaction between TAM receptor and type I IFN signaling, we treated *Ifnar*$^{-/-}$ BMECs with Gas6. Type I IFN signaling was not required for Gas-6-dependent effects on TEER at 30 and 60 minutes after treatment, although an absence of IFNAR diminished the amplitude of the effect at all time points (**Supplementary Fig 7a**). We confirmed these findings with MAR1-5A3[30], an IFNAR-blocking antibody, which was incubated with WT BMECs immediately prior to Gas6 addition (**Supplementary Fig 7b**). Thus, TAM receptor ligands activate Mertk to tighten the junctions of BMEC monolayers in a manner that cooperates with but does not require IFNAR signaling, and the effect of Mertk on endothelial barrier integrity is amplified when type I IFN signaling occurs concurrently.

We examined how Gas6-dependent TAM receptor signaling affected the activity of Rac1, a Rho family GTPase that regulates cytoskeletal dynamics, TJ integrity, and paracellular permeability[31]. IFN-β enhances BMEC barrier formation in part by activating Rac1[22], and Mertk signaling promotes Rac1 activation in macrophages in the context of phagocytosis of apoptotic debris[32]. We measured GTP-bound, activated Rac1 after treatment with IFN-β, Gas6, or IFN-β and Gas6. Notably, Gas6 treatment was sufficient to enhance Rac1 activation in BMECs, similar to the effect of IFN-β alone (**Fig 5f,** 2-fold, $P < 0.005$). The combination of Gas6 and IFN- β led to a further increase in Rac1 activation. Finally, blockade of Rac1 activation prevented Mertk- or IFN-β-dependent tightening of BMEC barriers (**Fig 5g**). Thus, cytoskeletal reorganization resulting from Gas6-induced activation of Rac1 is likely required to sustain TJ integrity and the endothelial barrier.

We evaluated Axl and Mertk expression in cells of the neurovascular unit by confocal microscopy (**Supplementary Fig 8a–b**). In addition to expression on endothelial cells (**Supplementary Fig 5a–c**), we observed co-staining of TAM receptors in S100β$^+$ astrocytes and CD11b$^+$ myeloid cells. To evaluate whether TAM receptor expression on astrocytes contributed to endothelial barrier integrity, using the *in vitro* BBB model, we tested whether the TEER response to Gas6 stimulation was different with WT versus *Axl*$^{-/-}$*Mertk*$^{-/-}$ astrocytes. However, deletion of Axl and Mertk in astrocytes had no effect on TEER (**Fig 6a**).

The effect of Mertk expression on BBB permeability occurred both *in vitro* and *in vivo*, without appreciable effects on viral replication in peripheral organs or on CD8$^+$ T cell responses. To confirm that the dominant effect on BBB permeability of Mertk occurred at the level of the neurovascular unit and not in peripheral immune cells, we generated Mertk bone marrow chimeric mice. To prevent adventitious effects of radiation on the BBB, the heads of mice were shielded with lead (**Fig 6b**). Bone marrow chimeras with Mertk-deficient radio-resistant non-hematopoietic cells (SJL→*Mertk*$^{-/-}$) exhibited the same BBB permeability defect on day 4 after WNV infection as *Mertk*$^{-/-}$ mice whereas the reciprocal chimeras (*Mertk*$^{-/-}$→SJL) with Mertk-sufficient non-hematopoietic cells did not (**Fig 6c**). A trend towards a parallel effect on viral burden was observed with 7 of 8 SJL→*Mertk*$^{-/-}$ mice having detectable WNV RNA in the brain at 4 dpi compared to 3 of 8 *Mertk*$^{-/-}$→SJL mice (**Fig 6d,** $P = 0.06$). These results are consistent with a model in which Mertk expression on radio-resistant cells within the CNS is required for maintenance of BBB integrity.

DISCUSSION

Many enveloped viruses bind to and activate TAM receptors to disable innate immune responses and enhance infection[19]. Because we previously observed slightly lower levels of WNV replication in *Axl*$^{-/-}$*Mertk*$^{-/-}$ DCs[19], we hypothesized that TAM receptor-deficient mice would be protected against lethal WNV infection. However, we show here that a genetic deficiency of Axl and Mertk resulted in the early appearance of WNV into the CNS, which resulted in enhanced viral load and mortality. The increased mortality was associated with increased BBB permeability and revealed a dominant role for Mertk in maintaining the integrity of this key barrier during viral infection. Using an *in vitro* BBB model, we found that Mertk promoted endothelial barrier integrity by maintaining the co-localization of TJ

proteins. The barrier-tightening effect of Mertk signaling was cooperative with the response to IFN-β.

Our discovery that *Axl*$^{-/-}$ and *Mertk*$^{-/-}$ mice were more vulnerable to neuroinvasive WNV and LACV infections suggests that although enveloped viruses can usurp TAM receptors, these proteins nonetheless can restrict the pathogenesis of some viruses that gain entry into the CNS. When WNV was introduced directly in the CNS by intracranial injection in TAM receptor-deficient animals, no increase in viral replication in different brain regions was observed. Thus, blockade or ablation of TAM receptors may have varying effects on viral pathogenesis depending on the balance between virus binding to TAM receptors via Protein S and/or Gas6 and the resulting effects on the intracellular antiviral environment and/or vascular endothelial barrier integrity. Our data also demonstrate a separate role of Axl in modulating T cell immunity, which could impact viral clearance in different tissues including the CNS.

Although we did not assay the level of infection in TAM-deficient DCs *in vivo*, peripheral viral burden was similar in WT, *Axl*$^{-/-}$, and *Mertk*$^{-/-}$ animals, suggesting that the earlier and greater viral burden in the CNS reflects accelerated virus entry due to impaired BBB integrity and that TAM receptor engagement by WNV is not required for infection *in vivo*. However, WNV infection was slightly greater in blood and the spleen of *Axl*$^{-/-}$*Mertk*$^{-/-}$ animals, the mechanism for which requires further study. Bone marrow chimera studies revealed that the BBB permeability phenotype tracked with a loss of Mertk expression on radio-resistant and not radio-sensitive hematopoietic cells. Mertk^{+} radio-resistant cells in the CNS also include microglia[33,34], which can express Axl upon activation; as such, we do not exclude the possibility that the enhanced lethality in WNV-infected *Axl*$^{-/-}$ mice might reflect a role for this TAM receptor in microglia.

IFNAR-dependent signaling was required for optimal endothelial cell barrier integrity after treatment with the TAM ligand, Gas6. Studies in myeloid cells have shown that Axl associates with and signals through the IFNAR1 subunit[11], and it is plausible that Mertk could function analogously in endothelial cells. Although biochemical corroboration is required, Mertk may modulate the barrier tightening effects of IFN-β in endothelial cells because of a specific interaction with IFNAR1[11].

The defects in the stabilization of endothelial TJs in *Axl*$^{-/-}$*Mertk*$^{-/-}$ BMECs are consistent with TAM receptor-dependent regulation of cytoskeletal reorganization in other cell types, which occur through Rac1[32,35]. We observed Rac1 activation in response to Gas6 in endothelial cells, which was amplified with concurrent IFN-β treatment. Our experiments are consistent with a model in which TAM receptor (preferentially Mertk) and IFNAR signaling together activate Rac1, which leads to tightening of BMEC junctions and restriction of virus transit into the CNS (**Fig 6e**).

Axl$^{-/-}$ mice had impaired CD8^{+} T cell responses to WNV infection, which could impact mortality by affecting CNS viral clearance[36,37]. We did not observe CD8^{+} T cell defects in peripheral or CNS tissues of *Mertk*$^{-/-}$ mice, suggesting distinct functions of Axl and Mertk in modulating adaptive immunity during virus infections. A diminished T cell response in

Axl$^{-/-}$ mice is consistent with a prior study of HSV infection [21]. However, the attenuated CD8^{+} T cell response does not explain the early appearance of WNV in the brain at day 4 in *Axl*$^{-/-}$ mice, since this time point precedes the induction of a WNV-specific CD8^{+} T cell response[38].

Prior reports have suggested possible functions of TAM receptors in endothelial cells. Mice lacking all three TAM receptors (*Axl*$^{-/-}$*Mertk*$^{-/-}$*Tyro3*$^{-/-}$ TKO) reportedly have a disrupted BBB, although this was attributed in part to autoimmune disease[39]. Exogenous administration of Protein S enhanced BBB integrity after ischemic stroke, although this phenotype required Tyro3 and not Axl or Mertk[26]. Thus, individual TAM receptors may have unique roles in maintaining BBB integrity under different inflammatory conditions. Mertk may have a dominant function in maintaining the BBB after viral infection, whereas Tyro3, which also is expressed on neurons, may be more important in the context of cerebral ischemia. Protein S, which is a ligand for both Tyro3 and Mertk, but not Gas6, is likely to be the relevant TAM ligand, as Protein S is abundant in serum where Gas6 is present at lower levels[40].

Our discovery that TAM signaling regulates BBB integrity in the context of viral infections has clinical implications, since TAM receptor antagonists are being developed as cancer therapies[41]. Mertk blockade could increase the risk of neuroinvasion and pathogenesis of certain viruses, including WNV and LACV. Indeed, in studies with a broad-spectrum inhibitor of TAM signaling[42], we observed increased lethality after WNV infection and increased BBB permeability. Further experiments are warranted to define the net effects of TAM receptor blockade in the context of infection by different families of visceral and encephalitic viruses.

ONLINE METHODS

Viruses and cells

The WNV strain (3000.0259) was isolated in New York in 2000 and passaged once in C6/36 *Aedes albopictus* cells. Mice were inoculated subcutaneously in the footpad with 10^2 plaque forming units (pfu) of WNV diluted in Hanks balanced salt solution. Viral titers in tissues were analyzed by plaque assay using Vero cells, as described previously. The LACV strain (original strain) was provided by Andrew Pekosz (Johns Hopkins University, Baltimore, Maryland, USA) and passaged twice in Vero cells to produce a virus stock.

Mice

C57BL/6J wild-type (WT) mice were commercially obtained from Jackson Laboratories. *Axl*$^{-/-}$, *Mertk*$^{-/-}$, *Axl*$^{-/-}$*Mertk*$^{-/-}$, and *Tyro3*$^{-/-}$ mice have been published[43] and were backcrossed for ten generations. All mice were housed in a pathogen-free mouse facility at the Washington University School of Medicine and experiments were performed in accordance with federal and University regulations. The protocols were approved by the Institutional Animal Care and Use Committee at the Washington University School of Medicine (Assurance Number: A3381-01). Mice (8 to 10 week-old, both sexes) were inoculated subcutaneously via footpad injection with 10^2 pfu of WNV or 10^5 focus-forming

units (ffu) of LACV, both diluted in 50 μl of Hanks balanced salt solution (HBSS) supplemented with 1% heat-inactivated fetal bovine serum (FBS). For intracranial infection, 10^1 pfu of WNV in 20 μl was injected into the right cerebral hemisphere.

Measurement of viral burden

At specified time points after WNV and LACV infection, serum was obtained by intracardiac heart puncture, followed by intracardiac perfusion (20 ml of PBS), and organ recovery. Organs were weighed, homogenized using a bead-beater apparatus, and WNV was titrated by plaque assay on Vero cells[44]. Brains from LACV- and WNV-infected mice were harvested at day 8 after infection and the total RNA was extracted using the RNeasy kit (Qiagen). For LACV, viral load in the brain was determined by qRT-PCR. Briefly, all reactions were assembled in a final volume of 25 μl with 300 ng of RNA, 10 μM forward and reverse primers (LACV: Forward 5'-CCTTGCTGCAGTTAGGATCTTCTT-3', Reverse 5'- CCACTCTCCAAATTTAGG-GTTAGC-3'; GAPDH: Forward 5'-AATGGTGAAGGTCGGTGTG-3', Reverse: 5'-GTG GAGTCATACTGGAACATGTAG-3'), 5 μM probe (LACV: 5'-5'-/56-FAM/ AGGCCAAGGCTGCTCTCTCGCGTA-/36-TAMSp/-3'; GAPDH: 5'-/56-FAM/ TGCAAATGG/ZEN/CAGCCCTGGTG/3IABkFQ/-3') and 12.5 μl of TaqMan master mix (Applied Biosystems) using the following cycling condition: 48°C for 30 min, 95°C for 10 min, followed by 45 cycles of 95°C for 15 s and 60°C for 1 min. Quantitation of WNV RNA was performed as previously described[45]. The levels of viral RNA were expressed on a $\log_{10}$ scale as genomes equivalents/g after comparison with a standard curve produced using serial ten-fold dilutions of WNV or LACV RNA.

Quantification of type I IFN activity

Levels of type I IFN were determined using an EMCV cytopathic effect bioassay performed in L929 cells as described previously[46]. Serum samples were treated with citrate buffer (40 mM citric acid, 10 mM KCl, 135 mM NaCl [pH 3.0]) for 10 minutes and neutralized with medium containing 45 mM HEPES pH 8.0. The amount of type I IFN per ml of serum was calculated from a standard curve using IFN-β (PBL Assay Science). The specificity of the antiviral activity was confirmed by pre-incubating L929 cells for 2 hours with 25 μg/ml of the IFNAR-blocking MAb MAR1-5A3 or an isotype control MAb GIR-208[30].

Cytokine bioplex assay

WT and *Axl*$^{-/-}$, *Mertk*$^{-/-}$, and *Axl*$^{-/-}$*Mertk*$^{-/-}$ mice were infected with WNV, and at specified times blood was collected and serum was prepared. The BioPlex Pro Assay was performed according to the manufacturer's protocol (BioRad). The cytokine screen included IL-1α, IL-1β, IL-2, IL-3 IL-4, IL-5, IL-6, IL-9, IL-10, IL-12p40, IL-12p70, IL-13, IL-17, Eotaxin, G-CSF, GM-CSF, IFN-γ, KC, MCP-1 MIP-1α, MIP-1β, RANTES (CCL5), and TNF-α.

BBB permeability measurements

Mice were infected with 10^2 pfu of WNV or diluent (mock) and BBB permeability was assessed after 4 days. Sodium fluorescein (100 mg/ml) was administered via an

intraperitoneal route in 100 μl. After 45 minutes, blood was collected by cardiac puncture into EDTA-coated tubes. Mice were perfused and CNS tissues were harvested, homogenized into PBS, clarified by centrifugation, precipitated in 1% trichloroacetic acid, and neutralized with borate buffer (Sigma-Aldrich). Fluorescence emission at 485 and 528 nm was determined using a microplate reader Synergy™ H1 and Gen5™ software (BioTek Instruments, Inc.). Fluorescein concentration was calculated from a standard curve and tissue fluorescence values were normalized to the plasma fluorescence values from the same mouse.

Endogenous mouse IgG was detected in brain sections using an AlexaFluor-488 anti-mouse IgG antibody. Nuclei were stained with Topro-3. Images were acquired with a laser scanning confocal microscope (Zeiss LSM 510 META) and analyzed with LSM image browser software (Zeiss).

Drug treatment studies

The small molecular receptor inhibitor BMS-777607 (Selleckchem) was dissolved in DMSO at a stock concentration of 52 mg/ml. Mice received either 1 mg BMS-777607 dissolved in 50 μl DMSO or 50 μl DMSO vehicle control by oral gavage beginning one day prior to infection and continuing through day 4 after infection.

B cell and antibody responses

The levels of WNV-specific IgM and IgG were determined using an ELISA against purified WNV E protein, as described previously[47]. Plaque reduction neutralization assays on BHK21-15 cells were performed after mixing serial dilutions of serum with a fixed amount (10^2 pfu) of WNV as previously described[48].

Cellular immune responses

WT and TAM receptor-deficient mice were infected in the footpad with 10^2 pfu of WNV and at 8 days after infection, spleens and brains were harvested after extensive cardiac perfusion with PBS. Splenocytes were dispersed into single cell suspensions with a cell strainer. Brains were digested collagenase and leukocytes were isolated as previously described[49]. Intracellular IFN-γ or TNF-α staining was performed after *ex vivo* restimulation with a D^b-restricted NS4B immunodominant peptide using 1 μM of peptide and 5 μg/ml of brefeldin A (Sigma) as described[50]. Cells were stained with the following antibodies and processed by multi-color flow cytometry on an LSR II flow cytometer (Becton Dickinson): CD3 (Becton Dickinson, clone 145-2C11), CD4 (Biolegend, clone RM4-5), CD8β (Biolegend, clone YT5156.7.7), CD19 (Invitrogen, clone 6D5), CD45 (Biolegend, clone 30-F11), CD11b (Becton Dickinson, clone M1/70), IFN-γ (Becton Dickinson, clone XMG1.2), TNF-α (Biolegend, clone MP6-XT22). Flow cytometry data were analyzed using FlowJo software (Treestar).

Transwell cultures and TEER measurements

WT and TAM receptor-deficient BMECs and WT HCMEC/D3 cells were grown until fully polarized in transwell cultures[22]. BMECs were grown above astrocyte cultures, whereas HCMEC/D3s were grown without astrocytes. TEER was measured via chopstick electrode

with an EVOM voltmeter (World Precision Instruments). Resistance values are reported as Ω/cm^2, with the resistance value for transwell inserts with no cells subtracted as background. TEER measurements were collected at 6 h following infection with WNV at MOI 0.01 or treatment with murine IFN-λ3 (100 ng/ml), murine or human IFN-β (10 ng/ml) (PBL Assay Science); mock wells were treated with culture medium. To block IFN-α/β signaling, BMEC cultures were treated with 25 μg/ml of the blocking MAb MAR1-5A3 for one hour prior to infection. A non-binding MAb (GIR-208) was used as an isotype control. To measure virus transit across the endothelial barrier, WNV was added to the upper chamber of the transwell at an MOI of 0.01. After 6 h, virus in the lower chamber was measured by qRT-PCR. Recombinant full-length Gas6 was generated in HEK293 EBNA cells as previously described[4]. Human Protein S was purchased from Haematologic Technologies (HCPS-0090).

Rac1 studies

Rac1 immunoprecipitation experiments were performed with an activated Rac1 agarose bead kit (Cell BioLabs, Inc.) according to the manufacturer's instructions. Purified, GTP-bound protein and unpurified BMEC protein lysates were separated via gel electrophoresis on 10% bis-Tris gels (Life Technologies) and transferred onto iBlot nitrocellulose transfer membranes (Life Technologies) according to standard protocols. To test the effects of Rac1 inhibition on TEER in BMECs, the Rac1 inhibitor Z62954982 (Cayman Chemical) was added at a concentration of 1 mM.

TAM receptor expression

Freshly isolated BMECs were stained with anti-Mertk (R&D Systems AF591) or anti-Axl (R&D Systems AF854) antibodies followed by a polyclonal secondary antibody. A control goat polyclonal antibody and $Axl^{-/-}Mertk^{-/-}$ BMECs were used to assess the specificity of staining. Brain sections were stained with antibodies against Mertk (R&D Systems, AF591), Axl (R&D Systems, AF854), s100-β (Abcam, ab41548), CD31 (Becton Dickinson, 550274), or CD11b (Becton Dickinson, ab8878).

Bone marrow chimeric mice

Six week-old B6.SJL-Ptprc (CD45.1 SJL, Jackson Laboratories) and CD45.2 $Mertk^{-/-}$ mice were anesthetized with ketamine and positioned within lead shielding to limit exposure of the brain to radiation[51]. Mice were then placed into a pie container within a cesium irradiator so that the head was shielded from the radiation source and then irradiated with a dose of 8 Gy. Six hours after irradiation, 10^7 bone marrow-derived leukocytes of a given genotype were injected intravenously in 100 μl of PBS. Seven weeks after bone marrow transplantation, reconstitution was confirmed by flow cytometry with greater than 95% of B cells, 90% of neutrophils, and ~75% of T cells of donor origin.

Power calculation and data generation

To determine mouse group sizes for individual experiments, power analysis was performed using the following values: probability of type I error = 0.05, power = 80%, 5-fold hypothetical difference in mean, and population variance. This analysis indicated that

minimum sample sizes of 8 animals for virological or immunological studies were required to detect an approximately 10-fold level of difference. Studies were performed in an unblended manner, and randomization was not used. No animals, samples, or data points were excluded from any analysis.

Data analysis

All data was analyzed using Prism software (GraphPad4, San Diego, CA). Kaplan-Meier survival curves were analyzed by the log rank test. Differences in viral burden, cytokine levels, and cell numbers were analyzed by the Mann-Whitney test.

Supplementary Material

Refer to Web version on PubMed Central for supplementary material.

ACKNOWLEDGMENTS

This work was supported by NIH grants U19 AI083019 (M.S.D. and R.S.K) and R01 AI101400 (M.S.D. and G.L.), R01 NS052632 (R.S.K.), and R01 NS085296 (G.L.). J.J.M. was supported by an NIH training grant, T32-AR007279 and a Rheumatology Research Foundation Scientist Development Award. B.P.D was supported by a National Science Foundation Graduate Research Fellowship (DGE-1143954) and NIH pre-doctoral fellowship (F31-NS07866). E.D.L was supported by postdoctoral fellowships from the Leukemia and Lymphoma Society and the Nomis Foundation.

REFERENCES

1. Lemke G. Biology of the TAM Receptors. Cold Spring Harbor Perspectives in Biology. 2013; 5:a009076. [PubMed: 24186067]
2. Cosemans JMEM, et al. Potentiating role of Gas6 and Tyro3, Axl and Mer (TAM) receptors in human and murine platelet activation and thrombus stabilization. Journal of Thrombosis and Haemostasis. 2010; 8:1797–1808. [PubMed: 20546121]
3. Prieto AL, Weber JL, Lai C. Expression of the receptor protein-tyrosine kinases Tyro-3, Axl, and Mer in the developing rat central nervous system. Journal of Comparative Neurology. 2000; 425:295–314. [PubMed: 10954847]
4. Lew ED, et al. Differential TAM receptor–ligand–phospholipid interactions delimit differential TAM bioactivities. eLife. 2014; 3:e03385.
5. Caraux A, et al. Natural killer cell differentiation driven by Tyro3 receptor tyrosine kinases. Nat Immunol. 2006; 7:747–754. [PubMed: 16751775]
6. Paolino M, et al. The E3 ligase Cbl-b and TAM receptors regulate cancer metastasis via natural killer cells. Nature. 2014; 507:508–512. [PubMed: 24553136]
7. Holland SJ, et al. R428, a Selective Small Molecule Inhibitor of Axl Kinase, Blocks Tumor Spread and Prolongs Survival in Models of Metastatic Breast Cancer. Cancer Research. 2010; 70:1544–1554. [PubMed: 20145120]
8. Holland SJ, et al. Multiple Roles for the Receptor Tyrosine Kinase Axl in Tumor Formation. Cancer Research. 2005; 65:9294–9303. [PubMed: 16230391]
9. Fraineau S, et al. The vitamin K–dependent anticoagulant factor, protein S, inhibits multiple VEGF-A–induced angiogenesis events in a Mer- and SHP2-dependent manner. 2012; 120:5073–5083.
10. Angelillo-Scherrer A, et al. Role of Gas6 receptors in platelet signaling during thrombus stabilization and implications for antithrombotic therapy. The Journal of Clinical Investigation. 2005; 115:237–246. [PubMed: 15650770]
11. Rothlin CV, Ghosh S, Zuniga EI, Oldstone MBA, Lemke G. TAM Receptors Are Pleiotropic Inhibitors of the Innate Immune Response. Cell. 2007; 131:1124–1136. [PubMed: 18083102]

12. Prasad D, et al. TAM receptor function in the retinal pigment epithelium. Molecular and Cellular Neuroscience. 2006; 33:96–108. [PubMed: 16901715]
13. Scott RS, et al. Phagocytosis and clearance of apoptotic cells is mediated by MER. Nature. 2001; 411:207–211. [PubMed: 11346799]
14. Zagorska A, Traves PG, Lew ED, Dransfield I, Lemke G. Diversification of TAM receptor tyrosine kinase function. Nat Immunol. 2014; 15:920–928. [PubMed: 25194421]
15. Sheridan C. First Axl inhibitor enters clinical trials. Nat Biotech. 2013; 31:775–776.
16. Graham DK, DeRyckere D, Davies KD, Earp HS. The TAM family: phosphatidylserine-sensing receptor tyrosine kinases gone awry in cancer. Nat Rev Cancer. 2014; 14:769–785. [PubMed: 25568918]
17. van den Brand BT, et al. Therapeutic efficacy of Tyro3, Axl, and Mer tyrosine kinase agonists in collagen-induced arthritis. Arthritis & Rheumatism. 2013; 65:671–680. [PubMed: 23203851]
18. Meertens L, et al. The TIM and TAM Families of Phosphatidylserine Receptors Mediate Dengue Virus Entry. Cell Host & Microbe. 2012; 12:544–557. [PubMed: 23084921]
19. Bhattacharyya S, et al. Enveloped Viruses Disable Innate Immune Responses in Dendritic Cells by Direct Activation of TAM Receptors. Cell Host & Microbe. 2013; 14:136–147. [PubMed: 23954153]
20. Shibata T, et al. Axl Receptor Blockade Ameliorates Pulmonary Pathology Resulting from Primary Viral Infection and Viral Exacerbation of Asthma. The Journal of Immunology. 2014; 192:3569–3581. [PubMed: 24659691]
21. Subramanian M, et al. An AXL/LRP-1/RANBP9 complex mediates DC efferocytosis and antigen cross-presentation in vivo. The Journal of Clinical Investigation. 2014; 124:1296–1308. [PubMed: 24509082]
22. Daniels BP, et al. Viral Pathogen-Associated Molecular Patterns Regulate Blood-Brain Barrier Integrity via Competing Innate Cytokine Signals. mBio. 2014; 5
23. Multiple Ascending Dose Study of BMS-777607 in Subjects With Advanced or Metastatic Solid Tumors.. ClinicalTrials.gov. 2015. https://clinicaltrials.gov/ct2/show/NCT00605618
24. McJunkin JE, et al. La Crosse Encephalitis in Children. New England Journal of Medicine. 2001; 344:801–807. [PubMed: 11248155]
25. Wang T, et al. Toll-like receptor 3 mediates West Nile virus entry into the brain causing lethal encephalitis. Nat Med. 2004; 10:1366–1373. [PubMed: 15558055]
26. Zhu D, et al. Protein S controls hypoxic/ischemic blood-brain barrier disruption through the TAM receptor Tyro3 and sphingosine 1-phosphate receptor. 2010; 115:4963–4972.
27. Chung W-S, et al. Astrocytes mediate synapse elimination through MEGF10 and MERTK pathways. Nature. 2013; 504:394–400. [PubMed: 24270812]
28. Brinton M. Replication Cycle and Molecular Biology of the West Nile Virus. Viruses. 2013; 6:13–53. [PubMed: 24378320]
29. Lazear HM, et al. Interferon lambda restricts West Nile virus neuroinvasion by enhancing integrity of the blood-brain barrier Science Translational Medicine. 2015
30. Sheehan KC, et al. Blocking monoclonal antibodies specific for mouse IFN-alpha/beta receptor subunit 1 (IFNAR-1) from mice immunized by in vivo hydrodynamic transfection. J Interferon Cytokine Res. 2006; 26:804–819. [PubMed: 17115899]
31. Etienne-Manneville S, Hall A. Rho GTPases in cell biology. Nature. 2002; 420:629–635. [PubMed: 12478284]
32. Mahajan NP, Earp HS. An SH2 Domain-dependent, Phosphotyrosine-independent Interaction between Vav1 and the Mer Receptor Tyrosine Kinase: A Mechanism for Localizaing Guanine Nucleotide-Exchange Factor Action. Journal of Biological Chemistry. 2003; 278:42596–42603. [PubMed: 12920122]
33. Gautier EL, et al. Gene-expression profiles and transcriptional regulatory pathways that underlie the identity and diversity of mouse tissue macrophages. Nat Immunol. 2012; 13:1118–1128. [PubMed: 23023392]
34. Ji R, et al. TAM Receptors Affect Adult Brain Neurogenesis by Negative Regulation of Microglial Cell Activation. The Journal of Immunology. 2013; 191:6165–6177. [PubMed: 24244024]

35. Tibrewal N, et al. Autophosphorylation Docking Site Tyr-867 in Mer Receptor Tyrosine Kinase Allows for Dissociation of Multiple Signaling Pathways for Phagocytosis of Apoptotic Cells and Down-modulation of Lipopolysaccharide inducible NF-κB Transcriptional Activation. Journal of Biological Chemistry. 2008; 283:3618–3627. [PubMed: 18039660]
36. Brien JD, Uhrlaub JL, Nikolich-Žugich J. Protective capacity and epitope specificity of CD8+ T cells responding to lethal West Nile virus infection. European Journal of Immunology. 2007; 37:1855–1863. [PubMed: 17559175]
37. Shrestha B, Diamond MS. Role of CD8+ T Cells in Control of West Nile Virus Infection. Journal of Virology. 2004; 78:8312–8321. [PubMed: 15254203]
38. Purtha WE, et al. Antigen-specific cytotoxic T lymphocytes pro lethal West Nile virus encephalitis. European Journal of Immunology. 2007; 37:1845–1854. [PubMed: 17559174]
39. Li Q, Lu Q, Lu H, Tian S, Lu Q. Systemic Autoimmunity in TAM Triple Knockout Mice Causes Inflammatory Brain Damage and Cell Death. PLoS ONE. 2013; 8:e64812. [PubMed: 23840307]
40. Burstyn-Cohen T, Heeb MJ, Lemke G. Lack of Protein S in mice causes embryonic lethal coagulopathy and vascular dysgenesis. The Journal of Clinical Investigation. 2009; 119:2942–2953. [PubMed: 19729839]
41. Verma A, Warner SL, Vankayalapati H, Bearss DJ, Sharma S. Targeting Axl and Mer Kinases in Cancer. Molecular Cancer Therapeutics. 2011; 10:1763–1773. [PubMed: 21933973]
42. Suárez RM, et al. Inhibitors of the TAM subfamily of tyrosine kinases: Synthesis and biological evaluation. European Journal of Medicinal Chemistry. 2013; 61:2–25. [PubMed: 22749189]
43. Lu Q, Lemke G. Homeostatic Regulation of the Immune System by Receptor Tyrosine Kinases of the Tyro 3 Family. Science. 2001; 293:306–311. [PubMed: 11452127]
44. Diamond MS, Shrestha B, Marri A, Mahan D, Engle M. B cells and antibody play critical roles in the immediate defense of disseminated infection by West Nile encephalitis virus. J Virol. 2003; 77:2578–2586. [PubMed: 12551996]
45. Samuel MA, et al. PKR and RNase L Contribute to Protection against Lethal West Nile Virus Infection by Controlling Early Viral Spread in the Periphery and Replication in Neurons. Journal of Virology. 2006; 80:7009–7019. [PubMed: 16809306]
46. Thackray LB, et al. Critical role for interferon regulatory factor 3 (IRF-3) and IRF-7 in type I interferon-mediated control of murine norovirus replication. J Virol. 2012; 86:13515–13523. [PubMed: 23035219]
47. Mehlhop E, Diamond MS. Protective immune responses against West Nile virus are primed by distinct complement activation pathways. J Exp Med. 2006; 203:1371–1381. [PubMed: 16651386]
48. Diamond MS, et al. A critical role for induced IgM in the protection against West Nile virus infection. J Exp Med. 2003; 198:1853–1862. [PubMed: 14662909]
49. Lazear HM, et al. Pattern Recognition Receptor MDA5 Modulates CD8+ T Cell-Dependent Clearance of West Nile Virus from the Central Nervous System. Journal of Virology. 2013; 87:11401–11415. [PubMed: 23966390]
50. Thackray LB, et al. Interferon regulatory factor 5 (IRF5)-dependent immune responses in the draining lymph node protect against West Nile virus infection. Journal of Virology. 2014; 88:11007–11021. [PubMed: 25031348]
51. Howell GR, et al. Radiation treatment inhibits monocyte entry into the optic nerve head and prevents neuronal damage in a mouse model of glaucoma. The Journal of Clinical Investigation. 2012; 122:1246–1261. [PubMed: 22426214]

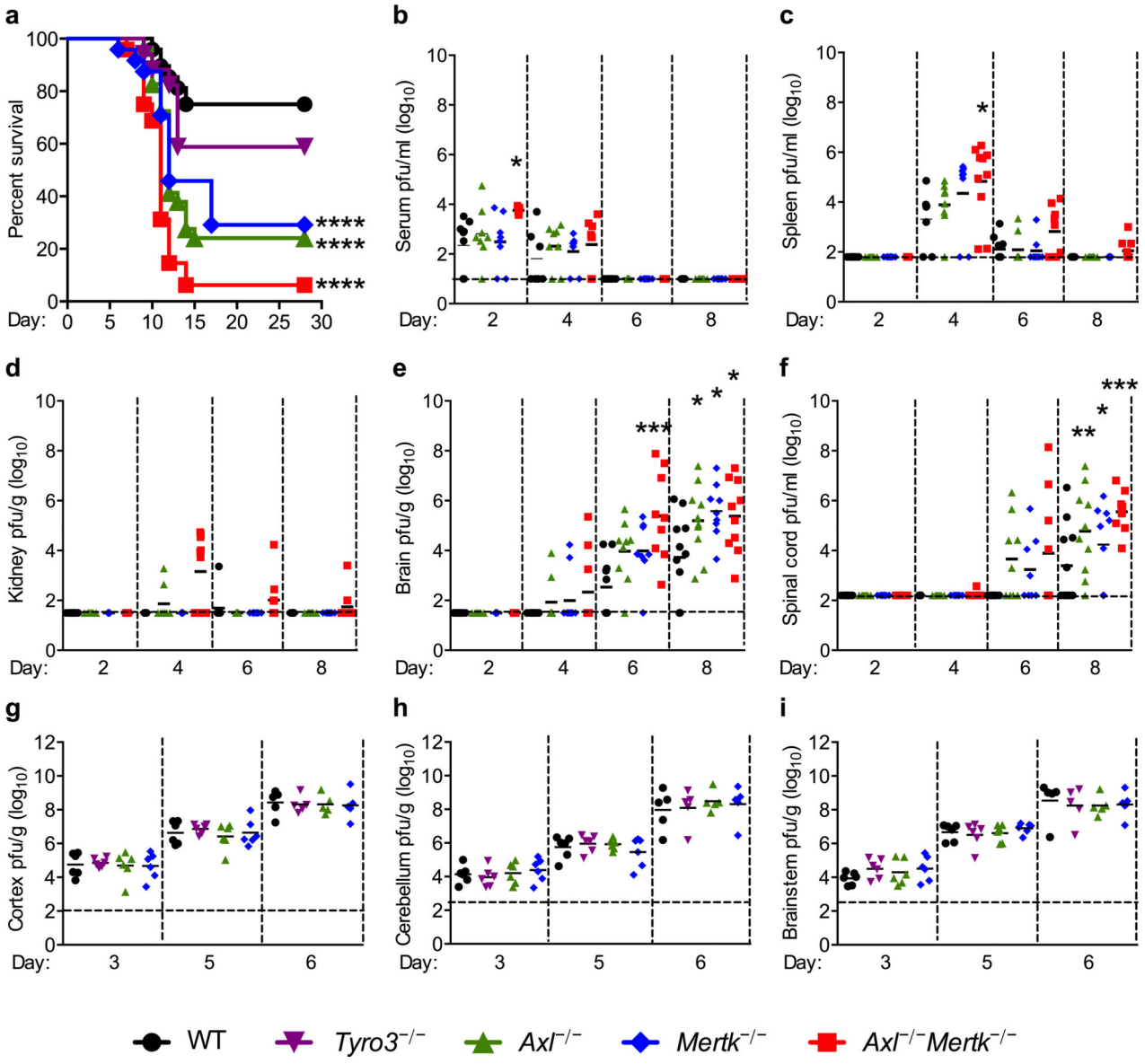

Figure 1. Mortality and viral burden in WT and TAM receptor-deficient mice after subcutaneous or intracranial infection with WNV

Mice were infected with 10^2 plaque forming units (pfu) of WNV via a subcutaneous route (**a–f**) or 10^1 pfu via an intracranial route (**g–i**). **a**. Survival analysis of WT, *Axl*$^{-/-}$, *Mertk*$^{-/-}$, *Tyro3*$^{-/-}$ and *Axl*$^{-/-}$*Mertk*$^{-/-}$ mice after subcutaneous WNV infection. Mice were monitored for 28 days for morbidity and mortality. The survival curves were constructed using data from three to five independent experiments. The survival differences between WT and *Axl*$^{-/-}$, *Mertk*$^{-/-}$, and *Axl*$^{-/-}$*Mertk*$^{-/-}$ mice were statistically significant by the log-rank test (****, $P < 0.0001$). The numbers of animals were $n = 49$ for WT, $n = 29$ for *Axl*$^{-/-}$, $n = 24$ for *Mertk*$^{-/-}$, $n = 17$ for *Tyro3*$^{-/-}$, and $n = 48$ for *Axl*$^{-/-}$*Mertk*$^{-/-}$. (**b–f**) Viral burden was measured by plaque assay from serum, spleen, kidney, brain, and spinal cord. Symbols represent individual mice pooled from several independent experiments; bars indicate the mean of 6 to 10 mice per group. Dotted lines represent the limit of sensitivity of the assay.

(**g–i**) Viral replication in the cerebral cortex, cerebellum, and brain stem was measured by plaque assay at days 3, 5, and 6 after infection. Bars indicate the mean of 5 or 6 mice per group from two independent experiments. Dotted lines represent the limit of sensitivity of the assay. *, $P < 0.05$; **, $P < 0.005$; ***, $P < 0.0005$; **** $P < 0.0001$ by the Mann-Whitney test.

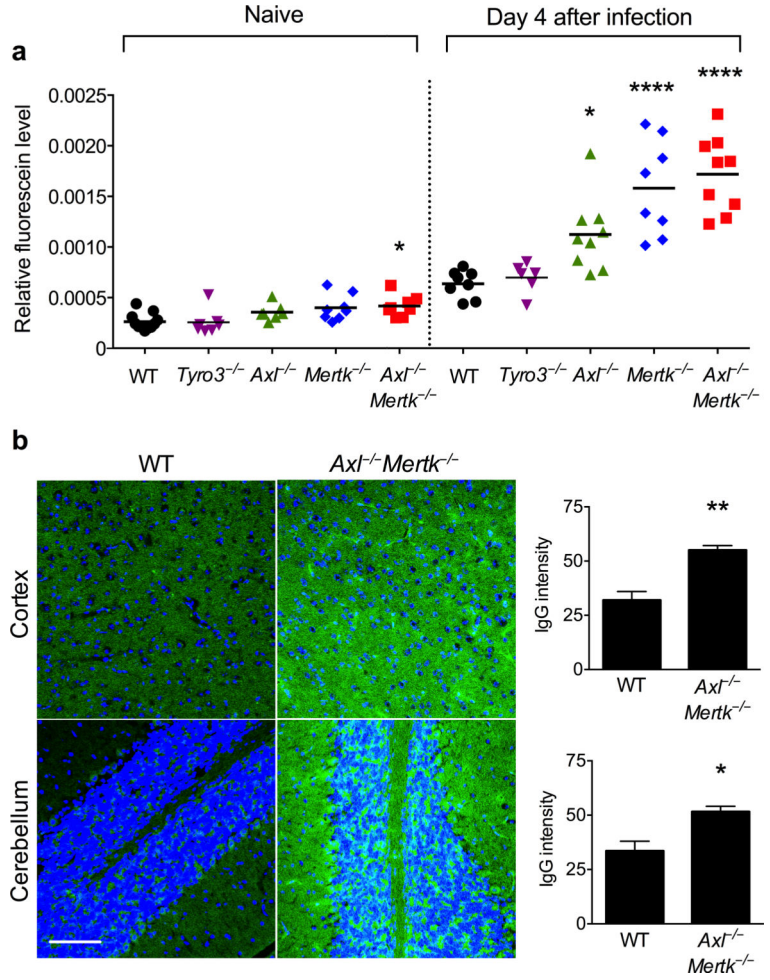

Figure 2. BBB permeability in WT and TAM receptor-deficient mice

(**a**) WT, *Axl*$^{-/-}$, *Mertk*$^{-/-}$, *Tyro3*$^{-/-}$ and *Axl*$^{-/-}$*Mertk*$^{-/-}$ mice were infected via a subcutaneous route with 10^2 pfu of WNV or diluent (mock). BBB permeability was assessed at 4 days after infection by measuring the accumulation of sodium fluorescein in CNS tissues following intraperitoneal administration. Tissue fluorescence was normalized to the plasma fluorescence from the same animal. Symbols represent individual animals from two independent experiments. ****, $P < 0.0001$; *, $P < 0.05$ (ANOVA with Tukey multiple comparisons test). (**b**) WT and *Axl*$^{-/-}$*Mertk*$^{-/-}$ mice were infected via a subcutaneous route with 10^2 pfu of WNV or diluent (mock). Mice were perfused and brain sections were stained with anti-mouse IgG to detect endogenous antibody leakage into the CNS parenchyma. IgG staining is shown in green, nuclei are shown in blue. Representative images were taken at 40X magnification. Scale bar equals 100 μm. Levels of IgG staining were quantified from 2 fields from 4 independent mice per group. *, $P < 0.05$ (Mann-Whitney test).

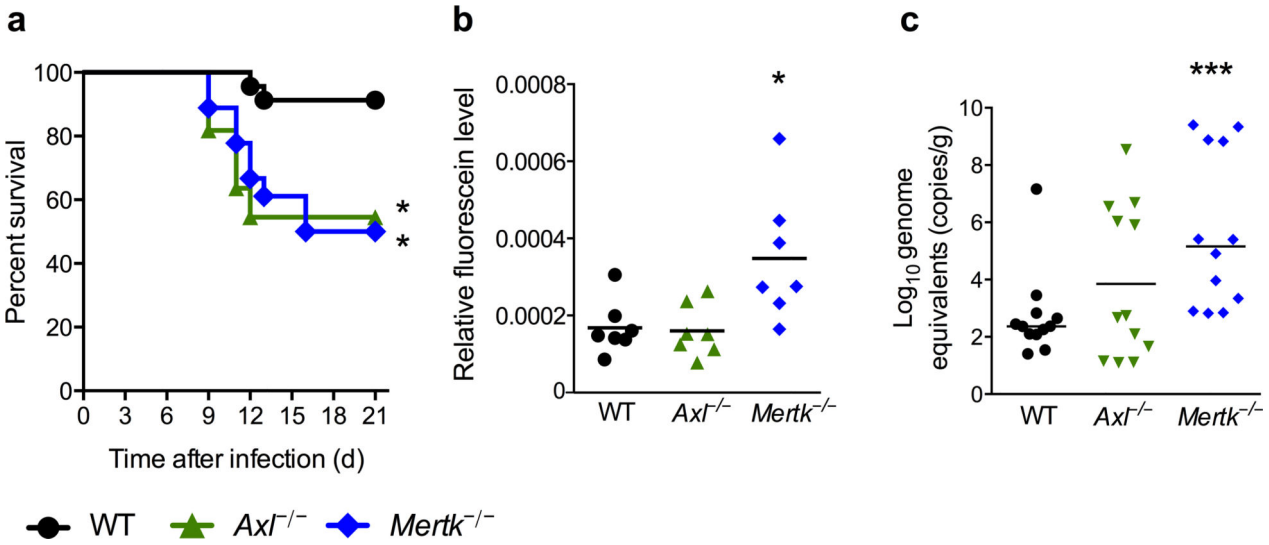

Figure 3. Vulnerability, viral burden, and BBB permeability in WT, *Axl*$^{-/-}$, and *Mertk*$^{-/-}$ mice after infection with LACV

8-week-old mice were infected with 10^5 focus forming units (ffu) of LACV via a subcutaneous route. (**a**) Survival analysis of WT, *Axl*$^{-/-}$, and *Mertk*$^{-/-}$ mice after LACV infection. The survival curves were constructed using data from three independent experiments and the differences between WT and *Mertk*$^{-/-}$ or WT and *Axl*$^{-/-}$ mice were statistically significant ($P < 0.05$) as judged by the log-rank test; $n = 23$ for WT, $n = 18$ for *Mertk*$^{-/-}$, $n = 11$ for *Axl*$^{-/-}$ mice. (**b**) BBB permeability was measured 4 days after infection by sodium fluorescein assay as described in legend to Figure 2. *, $P < 0.05$ (Mann-Whitney test). (**c**) Viral burden in the brain as measured by qRT-PCR and plotted as genome equivalents. $n = 12$ for WT, $n = 12$ for *Mertk*$^{-/-}$, and $n = 12$ for *Axl*$^{-/-}$ mice. ***, $P < 0.005$ (Mann-Whitney test).

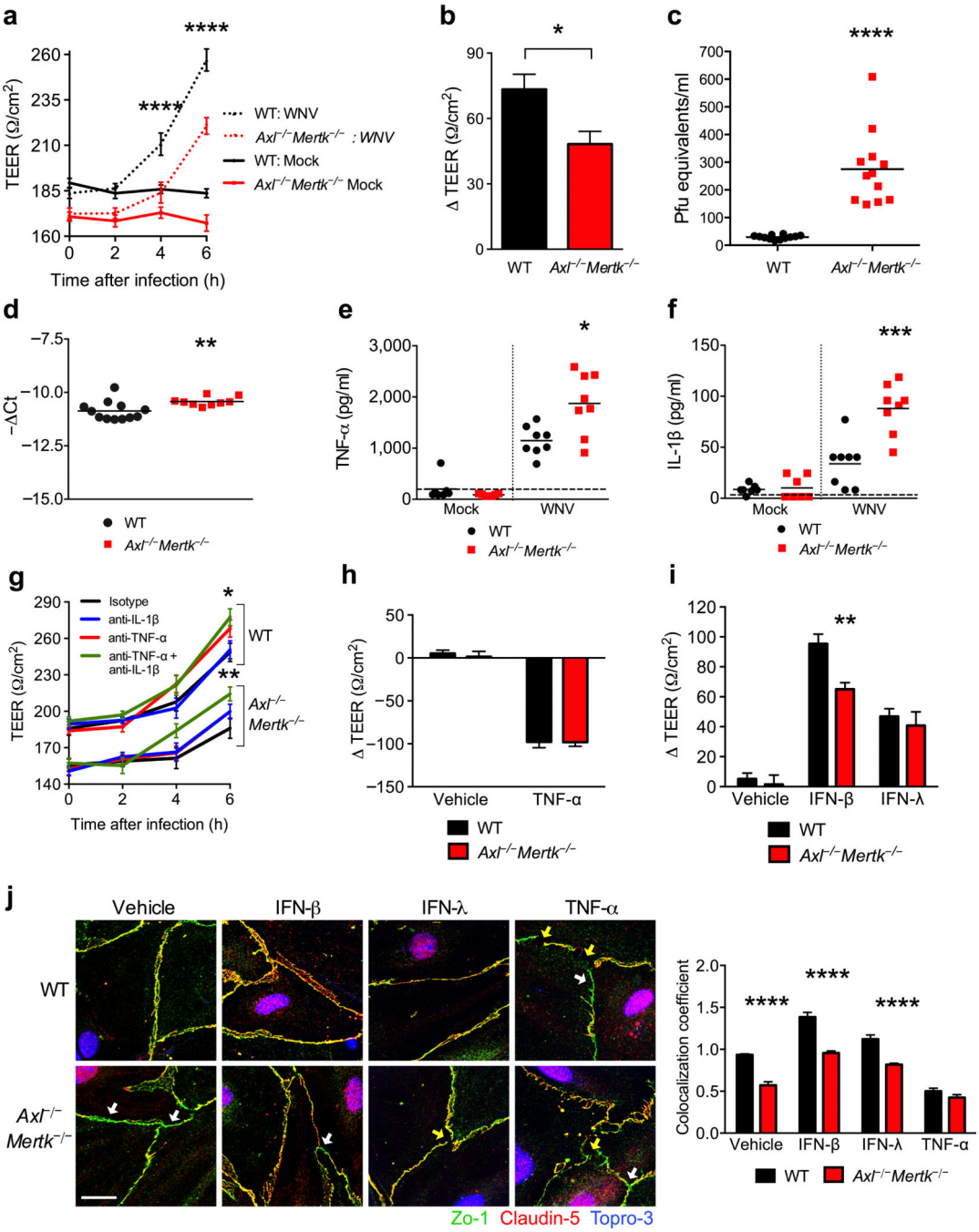

Figure 4. Analysis of barrier integrity in brain microvascular endothelial cells from *Axl*$^{-/-}$*Mertk*$^{-/-}$ mice

BMECs were prepared from WT or *Axl*$^{-/-}$*Mertk*$^{-/-}$ mice and cultured on transwell inserts with astrocytes prepared from WT mice. (**a**) BMECs were infected with WNV at an MOI of 0.01 and TEER was measured at two-hour intervals. (**b**) The relative changes in TEER over 6 h in WT and *Axl*$^{-/-}$*Mertk*$^{-/-}$ BMECs. (**c**) Virus crossing into the lower chamber of transwells with WT and *Axl*$^{-/-}$*Mertk*$^{-/-}$ BMECs measured by qRT-PCR and expressed as pfu equivalents/ml. (**d**) Measurement of WNV associated with WT and *Axl*$^{-/-}$*Mertk*$^{-/-}$

BMECs. Six hours after the addition WNV (MOI of 0.01), BMECs were rinsed six times and RNA was isolated and analyzed by qRT-PCR. (**e-f**) Cytokine levels in mock-infected and WNV-infected BMEC media were measured by Luminex assay. (**g**) WT and *Axl*$^{-/-}$*Mertk*$^{-/-}$ BMECs infected with WNV at a MOI of 0.01 were pre-treated with blocking antibodies to IL-1β and/or TNF-α and TEER was measured every 2 hours after infection for 6h. Results represent mean ± SEM of 9 samples from two independent experiments. ****, $P < 0.0001$; ***, $P < 0.0005$; **, $P < 0.005$, *, $P < 0.05$ (2-way ANOVA). (**h**) and (**i**) Cells were treated for 6 h with 100 ng/ml of TNF-α, 10 IU/ml murine IFN-β, or 100 ng/ml of murine IFN-λ3 for 6 h followed by TEER measurements. (**j**) BMECs were prepared from WT and *Axl*$^{-/-}$*Mertk*$^{-/-}$ mice and grown on chamber slides. Cells were co-stained for the TJ proteins ZO-1 (*green*) and claudin-5 (*red*); nuclei are shown in blue. Images were taken by confocal microscopy at 63X magnification. White arrows indicate diminished colocalization of ZO-1 and claudin-5. Yellow arrows indicate TJ discontinuities. Scale bar equals 25 μm. Right panel indicates the colocalization of claudin-5 and ZO-1. Values on the *y*-axis (correlation coefficient) represent the probability of an individual pixel staining positive for both markers if it stains positive for either. Results are representative of two or three independent experiments.

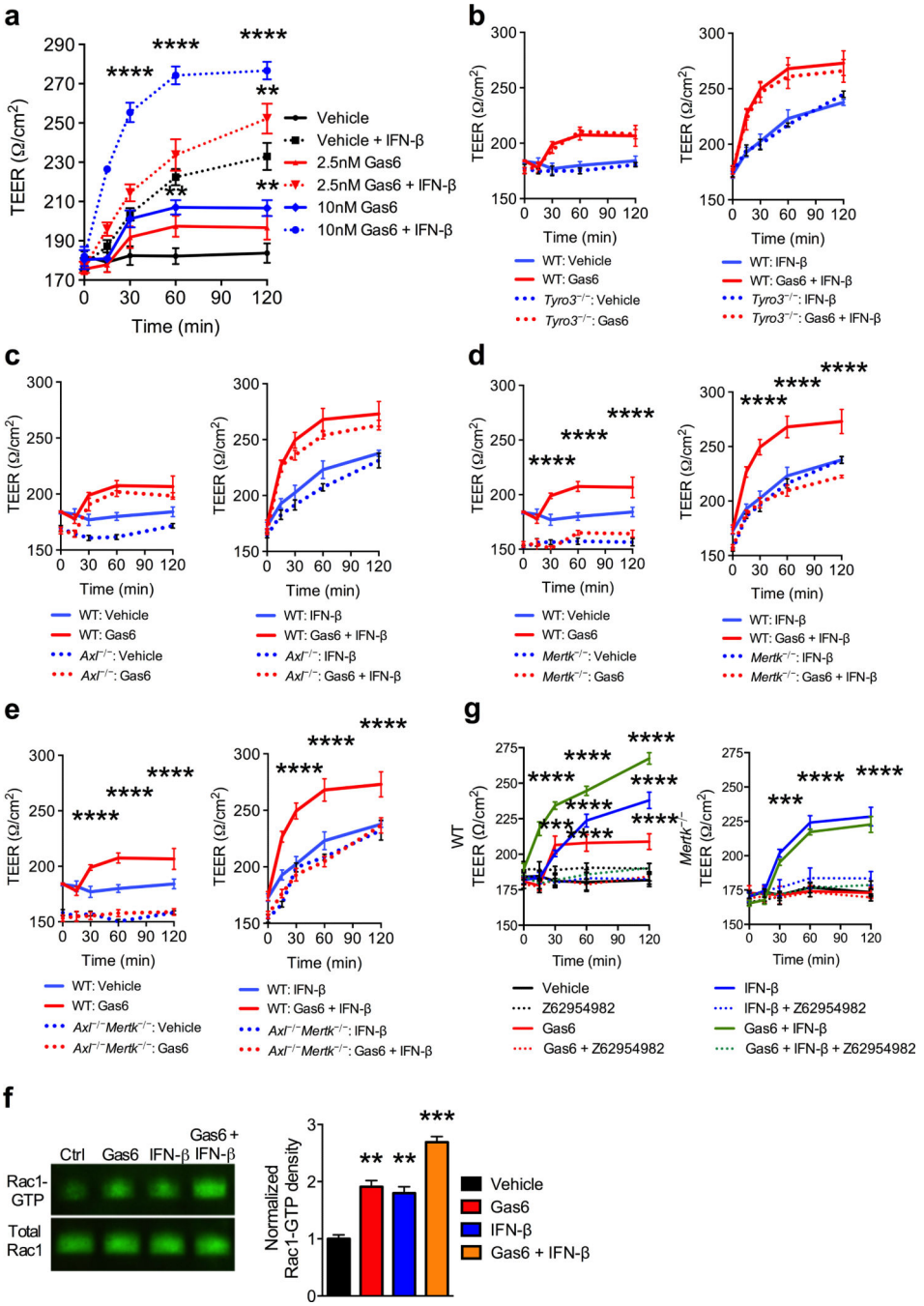

Figure 5. Mertk signaling tightens BMEC barriers and functions synergistically with IFN-β

BMECs were prepared from WT, *Axl*$^{-/-}$, *Mertk*$^{-/-}$, *Tyro3*$^{-/-}$, *Axl*$^{-/-}$*Mertk*$^{-/-}$ and *Ifnar1*$^{-/-}$ mice and cultured on transwell inserts with astrocytes prepared from WT mice. (**a**) Dose-dependent tightening of BMEC barrier integrity as measured by TEER in response to treatment with Gas6, IFN-β, or Gas6 + IFN-β. (**b–e**) TEER measurements after treatment of (**b**) *Tyro3*$^{-/-}$, (**c**) *Axl*$^{-/-}$, (**d**) *Mertk*$^{-/-}$ or (**e**) *Axl*$^{-/-}$ *Mertk*$^{-/-}$ BMEC monolayers with Gas6 (left panels) or IFN-β with or without Gas6 (right panels). (**f**) Rac1 activation as judged by immunoprecipitation after treatment of WT BMECs with Gas6, IFN-β, or Gas6 plus IFN-β.

The dose of Gas6 was 10 nM and the dose of IFN-β was 10 IU/ml. (**g**) TEER measurements after treatment of WT or *Mertk*$^{-/-}$ BMECs with Gas6, IFN-β, or Gas6 + IFN-β Gas6. Each group also was treated with the Rac1 inhibitor Z62954982 or with vehicle control. Results in this Figure are pooled from at least two independent experiments with 4 to 6 technical replicates. ****, $P < 0.0001$; ***, $P < 0.0005$; **, $P < 0.005$, *, $P < 0.05$ (2-way ANOVA).

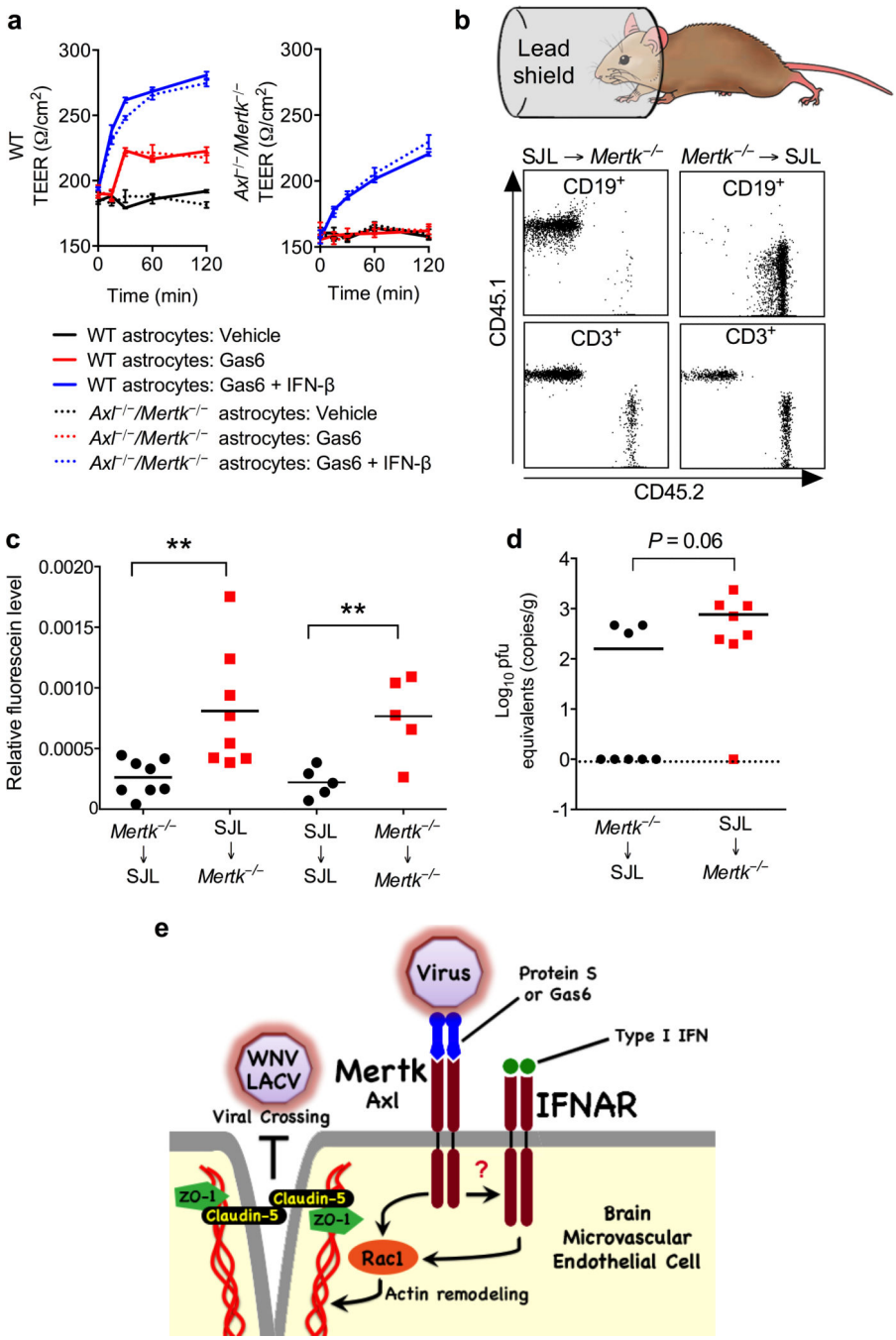

Figure 6. Enhanced BBB permeability occurs independently of Mertk expression on astrocytes and radiosensitive cells

(**a**) Dose-dependent tightening of WT and *Axl*$^{-/-}$*Mertk*$^{-/-}$ BMEC barrier integrity (grown over WT or *Axl*$^{-/-}$*Mertk*$^{-/-}$ astrocytes) as measured by TEER in response to treatment with Gas6, IFN-β, or Gas6 + IFN-β. (**b**) (*Top*) Scheme of head shielding of mice to prevent radiation damage to the BBB. (*Bottom*) Representative flow cytometry plots showing the reconstitution efficiency of CD19^{+} and CD3^{+} cells in *Mertk*$^{-/-}$ and SJL mice after bone marrow transplantation. (**c**) Sodium fluorescein measurement of BBB permeability in SJL→*Mertk*$^{-/-}$ and *Mertk*$^{-/-}$→SJL as well as control SJL→SJL and *Mertk*$^{-/-}$→*Mertk*$^{-/-}$

bone marrow chimeric mice 4 days after subcutaneous infection with 10^2 pfu of WNV; **, $P < 0.005$ (unpaired t test). (**d**) Measurement of WNV RNA in the brain by qRT-PCR on day 4 after infection; P = 0.06 (Mann-Whitney test). $n = 8$ for SJL→*Mertk*$^{-/-}$, $n = 8$ for *Mertk*$^{-/-}$→SJL, $n = 5$ for SJL→SJL, $n = 5$ for *Mertk*$^{-/-}$→*Mertk*$^{-/-}$ mice. (**e**) Model of cooperative IFNAR and TAM receptor signaling to activate Rac1, tighten the BBB, and prevent virus entry into the CNS. Signaling through Mertk and to a lesser extent Axl (via ligands Gas6 and Protein S) and IFNAR (via IFN-α/β) activate Rac1 within minutes, which leads to actin remodeling and stabilization of endothelial cell TJs. The question mark between TAM receptors and IFNAR indicates the uncertain mechanism by which IFN signaling modulates Mertk- and Axl-induced barrier tightening. Although experimental validation is required, a physical interaction between TAM receptors and IFNAR, as has been observed in DCs[11], could explain the observed phenotype.